THE IMPROVEMENT OF ARRAY ANTENNA PERFORMANCE WITH THE IMPLEMENTATION OF AN ARTIFICIAL MAGNETIC CONDUCTOR (AMC) GROUND PLANE AND IN-PHASE SUPERSTRATE

Raimi Dewan[1], Sharul K. A. Rahim[1, *], Siti F. Ausordin[1], and Teddy Purnamirza[1, 2]

[1]Wireless Communication Centre (WCC), Universiti Teknologi Malaysia, UTM Skudai, Johor 81310, Malaysia

[2]Department of Electrical Engineering, Faculty of Science and Technology, Universitas Islam Negeri Sultan Syarif Kasim, Pekan Baru, Indonesia

Abstract—This paper discusses performance improvement with the integration of an artificial magnetic conductor (AMC) into array antennas. An AMC with defected ground structure (DGS) was designed to construct the AMC ground plane and in-phase superstrate. The two distinguishable structures were integrated into an array antenna, which serves as a reference antenna at 5.8 GHz. The impedance bandwidth (BW) of the reference antenna significantly improved to 287% when integrated with an AMC ground plane and with 37% reduced size. On the other hand, the integration of in-phase superstrate effectively enhances the gain and BW of the reference antenna by 1 dBi and 44%, respectively. The effects of air gaps on the reference antenna with both the AMC ground plane and in-phase superstrate are discussed. The antenna performance factors, such as return loss and radiation pattern, are also discussed for the reference antenna, the reference antenna with the AMC ground plane, and the reference antenna with in-phase superstrate, respectively. There is satisfactorily good agreement between the simulation and measurement results. The proposed antenna is useful in WLAN (5.15–5.35 GHz and 5.725–5.825 GHz) and WiMAX (5.725–5.825 GHz) applications.

1. INTRODUCTION

Metamaterial is a composite material designed to mimic the specific characteristics [1] of materials that do not naturally exist [2, 3], such as perfect magnetic conductors (PMCs). The application of metamaterial has gained increasing attention in recent years due to this unique electromagnetic behavior [4, 5].

AMC is a class of metamaterial that exhibits the properties of the zero-degree reflection phase [6] of PMC at a resonant frequency. A perfect electric conductor (PEC) is typically used as a reflector to enable antenna radiation to focus in one direction. However, the use of PEC produces an image current that flows in the opposite direction relative to the original current. The image current will interfere with the original current, thereby attenuating or even cancelling the latter and consequently degrading the radiation efficiency. The attenuation can be reduced by separating the PEC surface from the antenna with a distance of $\lambda/4$. However, the penalty for reducing the attenuation is the increase in the overall antenna dimension; hence, the design will not be low-profile, which is a highly desirable characteristic for communication devices.

Interestingly, the image current problem can be solved by utilizing a PMC, which produces an image current in the same direction as that of the original current. This implies that the reflection phase is $0°$ and the magnitude of reflection coefficient, τ, equals +1. However, a PMC does not exist in nature, so an AMC can be designed only within a limited frequency band. AMC behaves like a PMC in the designed band, while it exhibits PEC characteristics in other bands [7]. AMC is closely related with the electromagnetic band gap (EBG), high impedance surfaces (HIS), and frequency selective surfaces (FSS).

Metamaterial is also used as a superstrate to improve antenna performance [8]. A metamaterial was used as the in-phase superstrate in [9], and it was placed on top of the antenna in a separate substrate, giving a zero reflection phase as PMC. The use of metamaterial can improve the flexibility in controlling the electromagnetic wave behavior of an antenna [10].

A microstrip antenna is a preferable choice in antenna design due to its low profile, low cost, ease of fabrication, and low weight and volume [11–13]. However, a microstrip antenna posses the drawbacks of low gain, narrow BW (typically 5%) [14, 15], and low efficiency and power [16]. Various research efforts have been and are still being made to improve microstrip antenna performance.

A BW enhancement (about 67%) was reported in [17], where the entire structure of a Jerusalem cross-shaped FSS was simulated with a

microstrip patch antenna resonating at 5.8 GHz. The simulation used the FSS dimensions as a variable and an invasive weed optimization approach, which is rather complex and time-consuming. The antenna BW was widened in [18], at 14.8 GHz, by integrating a dummy EBG structure at the antenna feed line. However, only 48.89% (0.381 GHz) BW was achieved compared to 0.256 GHz for the proposed reference antenna. Moreover, the use of a non-contacting technique also added to the fabrication complexity.

A miniaturized two-segment dielectric resonator antenna (TS-DRA) in [19] achieved a wide impedance BW of 14%. The trade off is the fabrication complexity in cutting and positioning the dielectric resonator to the feeding line to obtain a good impedance matching, return loss, and radiation pattern. In [20], the BW was increased from 10.1% to 19.9% at 5.2/5.8 GHz band by means of a ground stub. The difficulty encountered in obtaining a BW increase in the respective band is controlling the impedance matching. Adding to the complexity of the proposed design was the parasitic resonance caused by the coupling interaction between the ground stub and feeding line.

To the best of our knowledge, no analysis has been done on different AMC array positions on a dual-band array antenna. Hence, these papers provide study of a similar AMC design assigned at different positions when integrated with an array antenna: an AMC at the bottom of the array antenna as the AMC ground plane with the top of the array antenna as the in-phase superstrate. Additionally, the contribution also comes from the challenges of integrating the two structures into the array antenna instead of a single radiating patch antenna. This paper provides a basic study of comparison for both structures on the same array antenna design, which is used as a reference. Due to the simulated widening of bandwidth, the integrating structure capable of covering the bandwidth 5.15 to 5.875 GHz WLAN IEEE 802.11a [21] and the initially designed 5.8 GHz for WiMAX; for the case of AMC ground plane integrated with array antenna.

2. ARRAY ANTENNA AND AMC UNIT CELL DESIGN

The array antenna design was simulated using a transient solver in CST Microwave Studio 2010. A FR-4 was used as the substrate with a thickness of $h = 1.6\,\text{mm}$, copper thickness of 0.035 mm, dielectric permittivity of 4.3, and loss tangent of 0.0195. Figures 1(a)–(c) show the design sequence of the radiating patches of the array antenna. The conventional patch length L_P, and width, W_P, were initially approximated from the conventional antenna equation, such as in [15]. The L_P and W_P parameters will be used again for the dimension of the

array antenna in the case of integration with an AMC ground plane and an in-phase superstrate. Figure 1(a) shows the conventional patch with a feeding line. Next, the radiating patch is rotated 45° clockwise from the initial design, as shown in Figure 1(b). Finally, as shown in Figure 1(c), the chamfering is applied to the antenna on the left and right side as well as at the upper part of the radiating patch (labeled C_0 and C_1). An inset feed was applied to feed the radiating patch. The antenna design simply allows a further reduction in size of the radiating patch with the inclusion of the chamfering. The coordinate system is inserted in all related figures in this paper to facilitate a clear view of the design structures and radiation pattern.
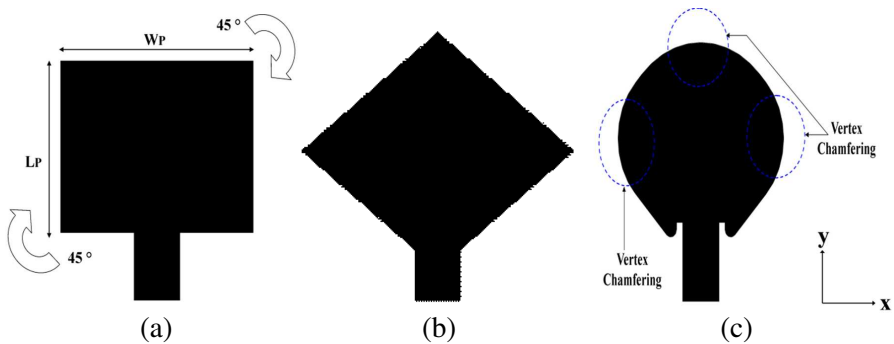

Figure 1. The design sequence of antenna radiating patches: (a) a conventional radiating patch, (b) the rotated radiating patch, and (c) the chamfering on the vertex of the rotated radiating patch.

Figure 2(a) shows the design of the array antenna with the substrate length and width labeled as *Ls* and *Ws*, respectively. The dimension's label on the array antenna will be used repeatedly in the following case of the array antenna with an AMC ground plane and an array antenna with an in-phase superstrate. However, the parameter value might not be the same for the three cases (except for the width and length of the substrate, which are set to be constant). Figure 2(b) shows the fabricated prototype of the array antenna. The transmission line of the particular impedance is labeled $T0$, $T1$, $T2$, and $T3$. The length and width of $T0$, $T1$, $T2$, and $T3$ are labeled L_{T0}, L_{T1}, L_{T2}, L_{T3}, and W_{T0}, W_{T1}, W_{T2}, W_{T3}, respectively. The coaxial connector with a core diameter of 1.0 mm is used to feed the antenna. The first transmission line, $T0$, is designed with a width W_{T0}, which is slightly bigger than the diameter of the core feeding. The simulated individual
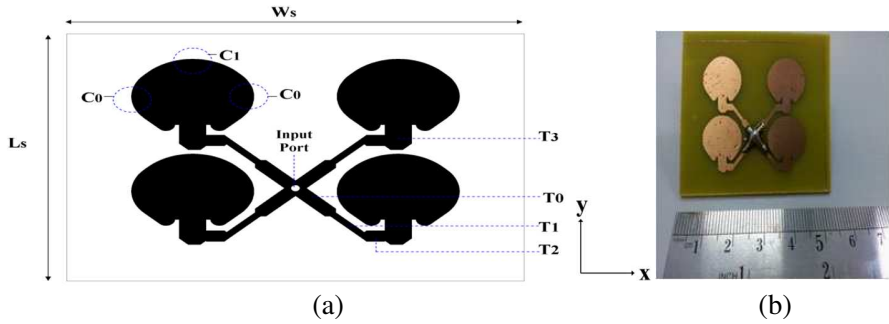
Figure 2. (a) The geometry of the array antenna and (b) the fabricated prototype. The antenna dimensions are $C_0 = 5.02$ mm, $C_1 = 7.00$ mm, $L_S = 40.06$ mm, $L_{T0} = 6.00$ mm, $L_{T1} = 5.40$ mm, $L_{T2} = 2.30$ mm, $L_{T3} = 4.05$ mm, $L_P = W_P = 12.70$ mm, $W_{T0} = 1.76$ mm, $W_{T1} = 0.88$ mm, $W_{T2} = 1.76$ mm, $W_{T3} = 3.04$ mm, and $W_S = 51.50$ mm.

area of the radiating patch was 1.61 cm^2. The array antenna herein will be treated as the reference antenna for the study of the AMC ground plane and in-phase superstrate.

The next step involves the design of the AMC unit cell. The conventional rectangular AMC, shown in Figure 1(a) of [6], is first initiated without any structure modifications, such as slots, rings, and so on. The design Equations (6)–(7) as in [17] were used to approximate the initial dimension of the AMC unit cell. The proposed design of the AMC unit cell integrated with DGS is shown in Figures 3(a)–(b); the substrate area and metalized copper layers are represented by the white and black shaded regions, respectively. The square-shaped AMC unit cell and defected ground structure (DGS) are similar in dimension except that each layer is a complete negative image of the other. In other words, when a square ring is printed on the top, the bottom layer is replaced with a square slot. The same applies to the design of the octagon ring, which resulted from the edge-chamfering of a square-shaped copper layer. This is done to minimize the metallization of AMC in the design's top layer. Figure 3(c) shows the three-dimensional (3D) view of the AMC unit cell. The spacing gap between each AMC unit cell is $g_{(d)}$.
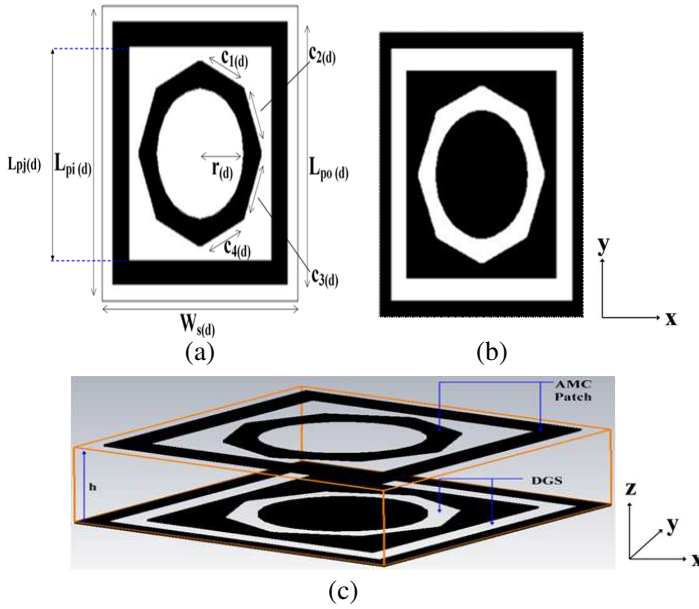
Figure 3. (a) The front view of the AMC, (b) the bottom view of the AMC (with DGS), and (c) the 3D view of AMC unit cell. AMC unit cell dimensions: $c_{1(d)} = 1.31\,\text{mm}$, $c_{2(d)} = 1.29\,\text{mm}$, $c_{3(d)} = 1.29\,\text{mm}$, $c_{4(d)} = 1.31\,\text{mm}$, $g_{(d)} = 0.62\,\text{mm}$, $L_{p0(d)} = 5.00\,\text{mm}$, $L_{pi(d)} = 5.62\,\text{mm}$, $L_{pj(d)} = 4.10\,\text{mm}$, and $r_{(d)} = 1.25\,\text{mm}$.

3. AMC GROUND PLANE AND IN-PHASE SUPERSTRATE INTEGRATED WITH ARRAY ANTENNA

An array antenna is located at the upper substrate, while an AMC ground plane is on a separate substrate positioned at the bottom layer of the array antenna. Figure 4(a) shows the geometry of the array antenna, while Figures 4(b)–(c) show the front and bottom design of the AMC periodic structure.

The array antenna was integrated with the AMC ground plane with an air gap of a mm. A non-conductive screw, E, with a diameter of d is used to hold the two substrate layers together. The coaxial connector of diameter D was used as the input feed to the antenna. Parameters $a = 0.5\,\text{mm}$, $d = 3.0\,\text{mm}$, $D = 1.0\,\text{mm}$, $t = 0.035\,\text{mm}$, and $h = 1.6\,\text{mm}$ are used in both the design of the array antenna with an AMC ground plane and the array antenna with an in-phase superstrate.
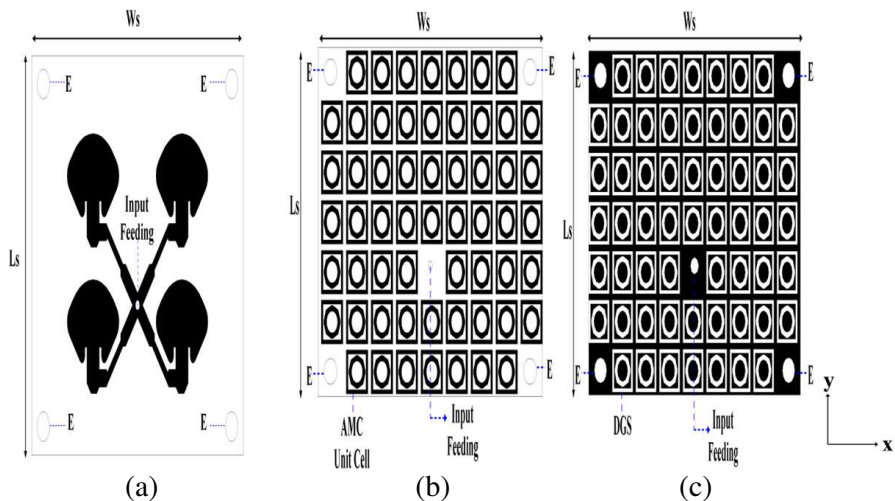
Figure 4. (a) The geometry of the array antenna at the top substrate, (b) the AMC periodic array, and (c) the DGS located at the bottom substrate. The antenna (with AMC ground plane) dimensions: $C_0 = 2.00\,\mathrm{mm}$, $C_1 = 7.00\,\mathrm{mm}$, $L_S = 40.06\,\mathrm{mm}$, $L_{T0} = 5.40\,\mathrm{mm}$, $L_{T1} = 5.40\,\mathrm{mm}$, $L_{T2} = 1.95\,\mathrm{mm}$, $L_{T3} = 4.64\,\mathrm{mm}$, $L_P = W_P = 10.10\,\mathrm{mm}$, $W_{T0} = 1.76\,\mathrm{mm}$, $W_{T1} = 0.88\,\mathrm{mm}$, $W_{T2} = 1.76\,\mathrm{mm}$, $W_{T3} = 3.04\,\mathrm{mm}$, and $W_S = 51.50\,\mathrm{mm}$.

The design of the AMC ground plane takes into account that the core feed of the coaxial connector was not connected to the ground layer of the bottom substrate and AMC patches; otherwise, the electromagnetic wave would be shortened and not propagate through the feeding network connected to the antenna radiating patch. The radius of the hole at the bottom structure was designed with a diameter greater than the diameter of the core of coaxial connector. The AMC patches were not located in the area where the core is located to avoid the aforementioned issue. t and h are the thickness of the copper layer and the substrate, respectively.

The core feed length is equivalent to the effective thickness of the overall integrated structure of the antenna with the AMC ground plane, which is $2h + 3t + a$. A longer core feed length will affect the antenna performance since a portion of the electromagnetic current will propagate through the tip of the core feed, reducing the total electromagnetic current supplied to the radiating patches.

Figure 5(a) shows the 3D design of the array antenna with an integrated AMC ground plane for a clear view of the overall

structure, while Figure 5(b) shows the fabricated prototype. The grey and transparent green line structure is the conductive layer and the substrate used, respectively. The simulated individual area of the radiating patch was $1.02\,\text{cm}^2$ for the case of AMC ground plane integrated with array antenna which is 37% smaller than the reference antenna.

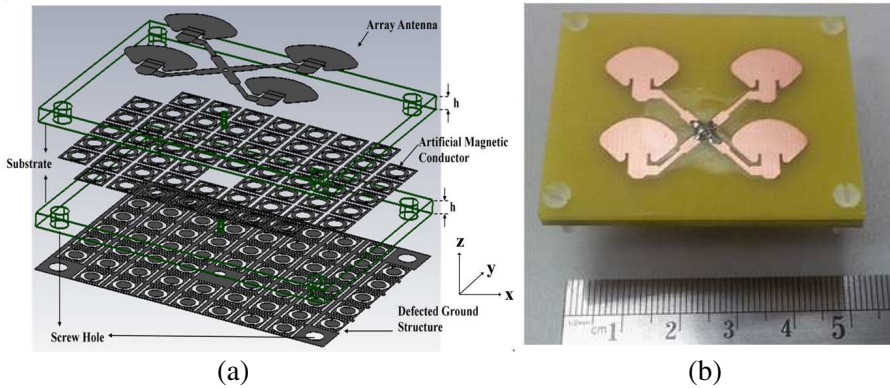(a)   (b)

Figure 5. (a) The exploded 3D view of the array antenna integrated with the AMC ground plane and (b) the fabricated prototype.

The next step was to design an array antenna integrated with an in-phase superstrate. The array antenna was located at the bottom substrate, while the in-phase superstrate was positioned at the top substrate of the array antenna, separated by an air gap of a mm. A non-conductive screw, E, with a diameter of d was used to hold the two substrate layers together. A coaxial connector of diameter D was used as the input feed to the antenna. The core feed length is $2h + t$ mm, while the overall structure thickness is $2h + 4t + a$ mm. The overall thickness of the array antenna integrated with the in-phase superstrate is greater than the thickness of the array antenna with the AMC ground plane by t mm. Figure 6(a) shows the geometry of the array antenna, while Figures 6(b)–(c) show the front and bottom design of the AMC periodic structure. Figures 7(a) and (b) show the 3D design of the array antenna integrated with the in-phase superstrate and the fabricated prototype, respectively. The simulated individual area of the radiating patch was $1.74\,\text{cm}^2$ for the case of in-phase superstrate integrated with array antenna which is slightly 8% larger than the reference antenna.

The air gap of $0.5\,\text{mm}$ in the AMC ground plane and in-phase superstrate with an array antenna was realized with the use of a non-
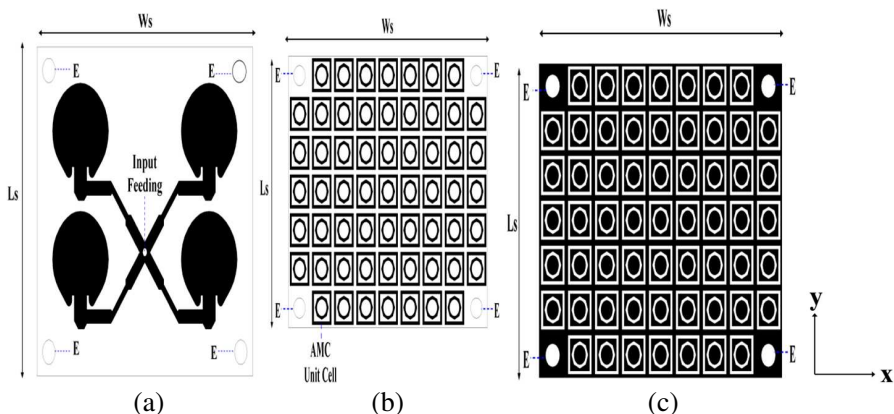
Figure 6. (a) The geometry of the array antenna at the bottom substrate, (b) the AMC periodic array, and (c) DGS located at the top substrate. The antenna (with in-phase superstrate) dimensions: $C_0 = 5.02$ mm, $C_1 = 7.00$ mm, $L_S = 40.06$ mm, $L_{T0} = 6.00$ mm, $L_{T1} = 5.40$ mm, $L_{T2} = 2.30$ mm, $L_{T3} = 3.94$ mm, $L_P = W_P = 13.20$ mm, $W_{T0} = 1.76$ mm, $W_{T1} = 0.88$ mm, $W_{T2} = 1.76$ mm, $W_{T3} = 3.04$ mm, and $W_S = 51.50$ mm.
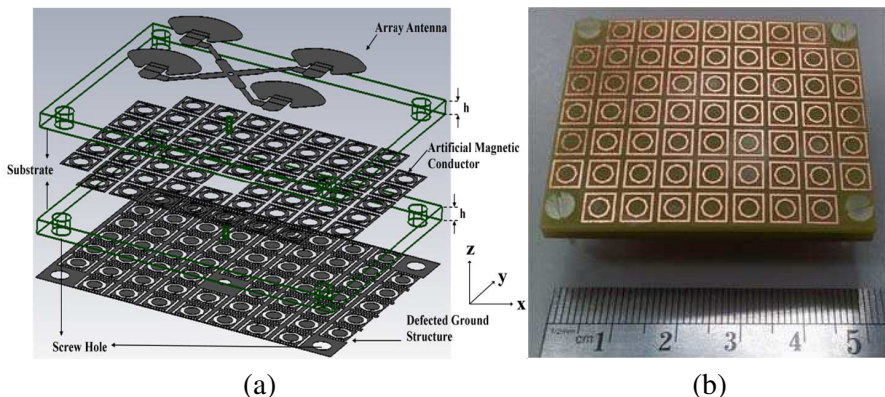

Figure 7. (a) The exploded 3D view of the array antenna integrated with the in-phase superstrate and (b) the fabricated prototype.

conductive material that is a cut square-shaped paper with a circular hole with a diameter of d. Figure 8(a) shows the thickness of the paper to be 0.5 mm using a Vernier caliper. The width of the paper is 5.0 mm, as shown in Figure 8(b). Figure 8(c) shows the measurement of the width of the stacked paper of about 5.05 mm. The thick paper is sandwiched between of the upper and bottom substrate, which is
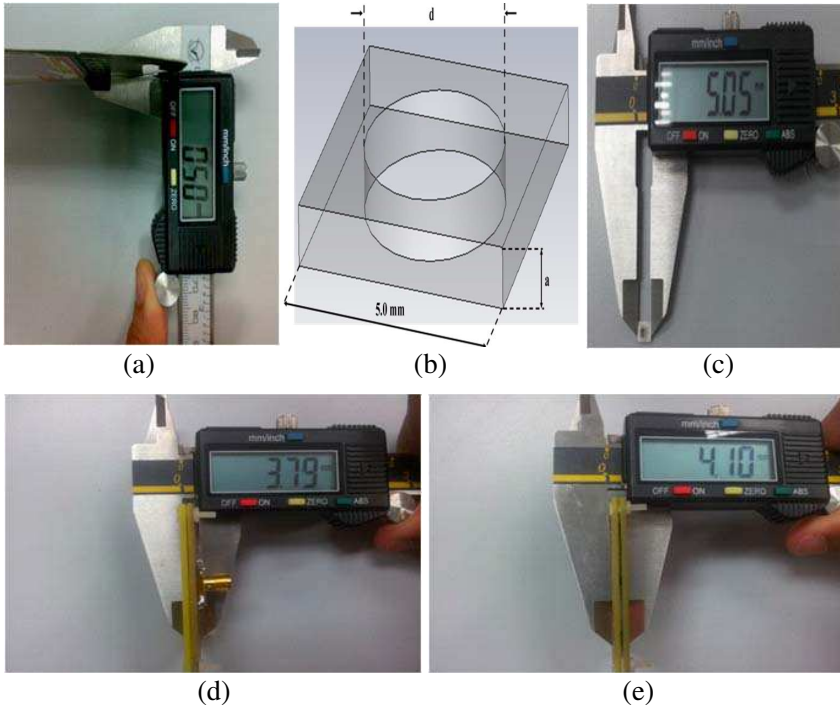
Figure 8. (a) Measurement of paper thickness, (b) paper geometry, (c) measurement the width of the stacked paper, measuring the overall thickness of the AMC ground plane with an array antenna, and (d) measurement of the overall thickness of the in-phase superstrate with an array antenna.

located at each corner of the rectangular substrate in parallel with the hole of the screw, as shown in Figures 8(d)–(e) for the AMC ground plane with an array antenna and an in-phase superstrate with an array antenna, respectively.

4. RESULTS AND DISCUSSION

In this section, the results of the reflection phase for the AMC with DGS are initially discussed. Next, parametric studies involving an array antenna with an AMC ground plane and an array antenna with an in-phase superstrate are analyzed, followed by a presentation of the results of the array antenna. Subsequently, simulated and measured results of the array antenna with the AMC ground plane and the array

antenna with an in-phase superstrate, respectively, are analyzed.

The proposed AMC with DGS and without DGS was designed to operate at a resonance frequency, f_r, of 5.8 GHz. This resonance frequency is the point where the AMC mimics the behavior of the zero degree reflection phases of perfect magnetic conductor (PMC) characteristics, which does not naturally exist. The conventional AMC unit cell design does not have any modification to its bottom structure. Here, we proposed the integration of DGS at the bottom of the AMC unit cell to widen the typically narrow bandwidth of AMC [22]. From Figure 9, it is observed that the integration of DGS successfully improves the bandwidth compared to the same AMC unit cell without the integration of DGS. The high frequency, f_H, and low frequency, f_L, are located at $-90°$ and $90°$, respectively, for the AMC with integrated DGS. The high frequency, f_h, and low frequency, f_l, are located at $-90°$ and $90°$, respectively, for the AMC without integrated DGS. The percentage bandwidth of the AMC with and without DGS is 26.63% and 15.64%, respectively. Both of them have higher-percentage bandwidth that the percentage bandwidth in reference [23, 24] that operates at a similar frequency. The AMC bandwidth is enhanced so that, when integrated with a microstrip antenna, the widening impedance bandwidth of the antenna can be maximized.
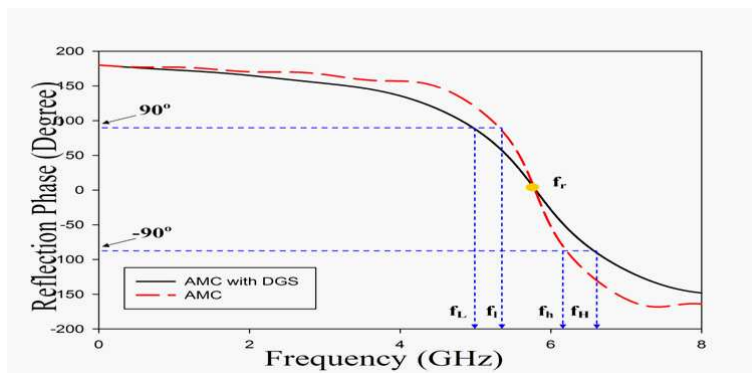

Figure 9. The simulated variations of the reflection phase of the AMC with and without DGS.

Figure 10(a) shows the parametric studies of air gaps in the array antenna with the AMC ground plane. A 10 dB return loss curve cannot be obtained with an air gap of 1.0 mm, 1.5 mm, or 2.0 mm within the range of 4–7 GHz. A 10 dB return loss curve is successfully achieved within the frequency range for an air gap of 0 mm and 0.5 mm. However, a 10 dB return loss is not achieved at the intended operating

frequency of 5.8 GHz for air gap of 0 mm. Hence, the value of 0.5 mm is chosen as the air gap between the array antenna and the AMC ground plane. The 0.5 mm distance is equivalent to $\lambda/100$ with respect to 5.8 GHz.

Figure 10(b) shows the parametric studies on the air gap for the array antenna with an in-phase superstrate. Similarly to the array antenna with the AMC ground plane, the air gaps of 0 mm, 0.5 mm, 1.0 mm, 1.5 mm, and 2.0 mm were chosen for the case of the array antenna with the in-phase superstrate. Within the range of 4–7 GHz, a 10 dB return loss curve cannot be achieved for the air gap value of 0 mm and 2.0 mm. The air gap of 1.0 mm achieved exactly 10 dB of return loss at 5.8 GHz, which is not an appropriate value for fabrication. A fabrication fault might occur, causing the fabricated prototype to fail to perform the exact 10 dB return loss at 5.8 GHz as in the simulation. The air gaps of 0.5 mm and 1.5 mm exhibit a satisfactory return loss curve. The air gap of 0.5 mm was chosen instead of 1.5 mm to reduce as much as possible the overall thickness of the structure of the array antenna with the in-phase superstrate.

The design of multiple substrate structures is challenging due to the effect of the air gap that separates the top and bottom substrates. The air gap can significantly affect the antenna performance. The design of structures with air gaps also contributes to the fabrication
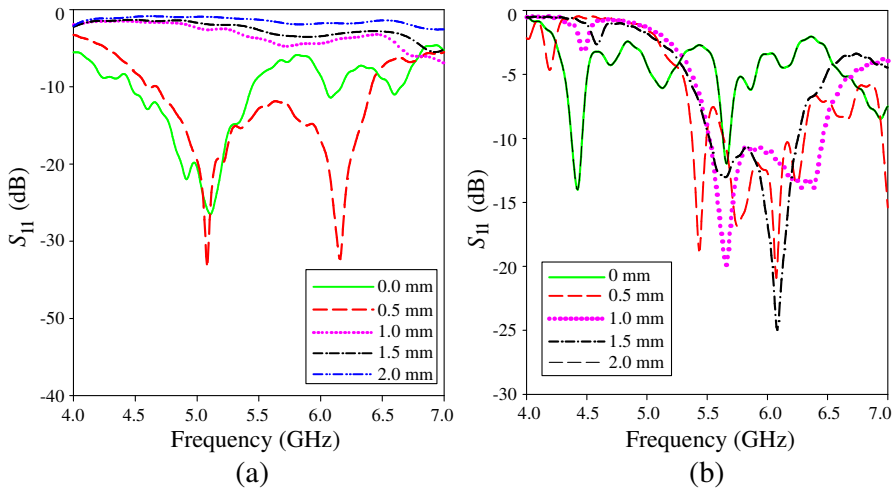

Figure 10. The simulated variations of return loss with respect to the air gap in an array antenna: (a) integrated with AMC ground plane and (b) integrated with an in-phase superstrate.

complexity. The practical value of the air gap needs to be chosen to minimize the fabrication complexity as much as possible.

Figure 11 shows a parametric study of the air gap versus the gain of the array antenna with the AMC ground plane and the array antenna with the in-phase superstrate at 5.8 GHz. It can be seen from both structures that the gain is at its lowest when the air gap is 0 mm. The gain value then gradually increases from 0 up to the maximum value at an air gap of 0.5 mm for the array antenna with the AMC ground plane and the array antenna with the in-phase superstrate. The gain decreases for the subsequent values of air gaps greater than 0.5 mm. The antenna with the in-phase superstrate gives a higher gain than the array antenna with an AMC ground plane with a difference of 1.67 dBi. The air gap limits the value of the gain in the array antenna with the AMC ground plane to a maximum value of 5.61 dBi, which is 0.65 dBi lower than the gain of the reference antenna. Conversely, in the case of the array antenna with an in-phase superstrate, the addition of the structure to the antenna increases the gain to 7.27 dBi, which is 1.04 dBi higher than the gain of the reference antenna.
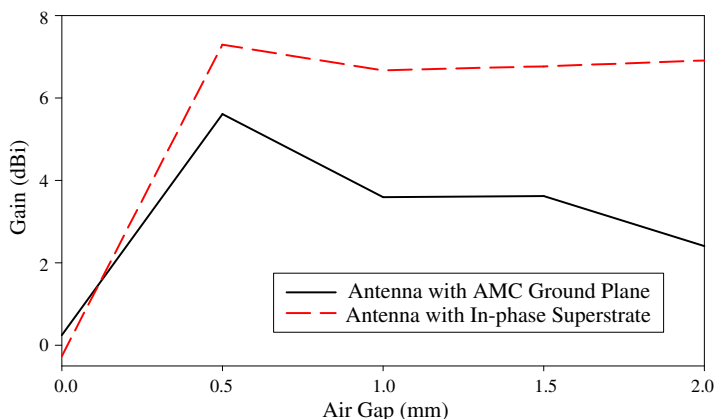

Figure 11. The simulated variations of gain with respect to the air gap in an array antenna integrated with the AMC ground plane and an array antenna with an in-phase superstrate.

Figure 12 shows the simulated and measured return loss of the array antenna. The measured results agree satisfactorily with the simulated result with a slight shift to the right. The higher frequency, f_{high}, and lower frequency, f_{lower}, are 5.90 GHz and 5.45 GHz, respectively. The corresponding simulated bandwidth is 0.45 GHz. Table 1 shows the detailed performance of the array antenna.
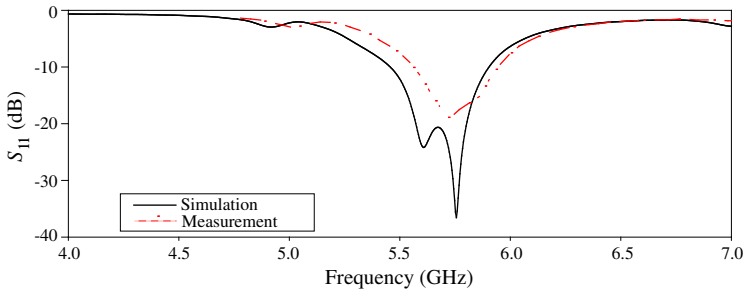
Figure 12. The simulated and measured results of the return loss curve for the array antenna.
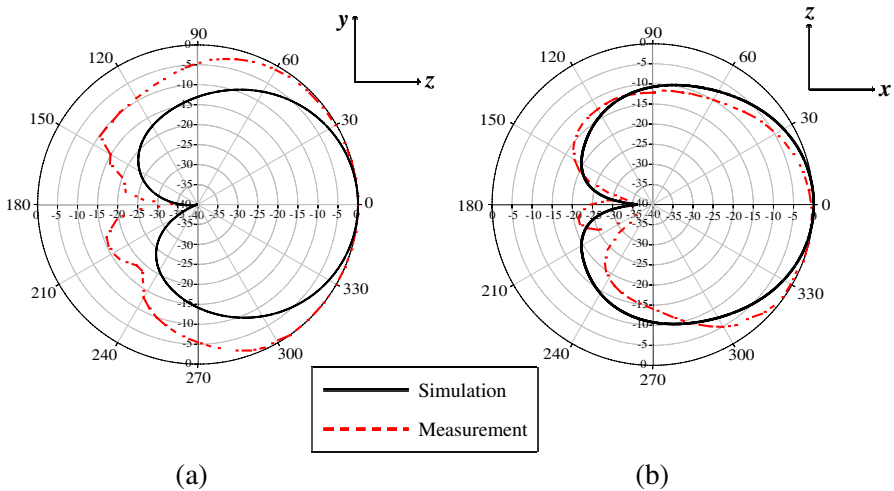

(a)   (b)

Figure 13. The simulated and measured results of the radiation pattern of the array antenna for the (a) E-field and (b) H-field, respectively.

Figures 13(a) and (b) show the results of the radiation pattern of the array antenna for the E-field and H-field, respectively. The array antenna has a maximum gain of 6.26 dBi in the direction of $0°$ with half-power beam widths (HPBW) of $71.5°$. It can be observed that the measured radiation pattern follows a similar shape to that of the simulated one.

Figure 14(a) shows the simulated and measured results of return losses for the array antenna with the AMC ground plane. The higher frequency, f_{hi}, and lower frequency, f_{low}, are 6.41 GHz and 4.67 GHz,

respectively which correspond to simulated bandwidth of 1.74 GHz. Table 1 shows the detailed performance of the array antenna with the AMC ground plane. It can be seen that, with the integration of the AMC ground plane into the array antenna, the impedance bandwidth of the array antenna has been widened by as much as 287% compared to the reference antenna. Equation (1) was used to calculate the improvement in bandwidth whereby the initial bandwidth was based on the bandwidth of the reference antenna. The initially operated array antenna at 5.8 GHz is capable of operating in the 5.2 GHz band due to the widening of the impedance bandwidth. A study of the radiation pattern was carried out at 5.2 GHz and 5.8 GHz. However, it can be observed that, at lower bandwidths, the measured return loss curve bulges at 5.0 GHz compared to the simulated one. The lower resonance, which is the 5.2 GHz band, exists due to the entire simulated structure of the array antenna and AMC ground plane with a controlled air gap. However, in the fabrication, a precise air gap is difficult to achieve at every point between the top substrate and the bottom substrate, which affects the loss of the array antenna. Therefore, for the fabricated prototype, the antenna can only covered the WLAN band at 5.725–5.825 GHz.

$$\%\text{Bandwidth improvement} = \frac{\text{New bandwidth} - \text{Initial bandwidth}}{\text{Initial bandwidth}} (100\%) \quad (1)$$

where the new bandwidth was based on the simulated bandwidth of AMC ground plane or In-phase superstrate with array antenna.
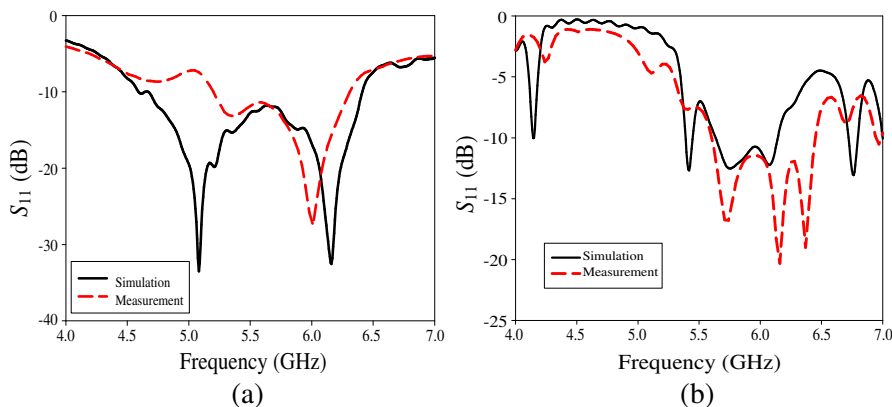

Figure 14. (a) The simulated and measured results of the return loss curve for the array antenna with the AMC ground plane and (b) the simulated and measured results of the return loss curve for the array antenna with the in-phase superstrate.

A similar case occurs with the return loss results shown in Figure 14(b) for the array antenna with the in-phase superstrate. Although the measured result has an approximately similar shape with the simulated one, the measured bandwidth is greater than the simulated one. The higher frequency, f_{hc}, and lower frequency, f_{lc}, are 6.30 GHz and 5.65 GHz, respectively, which correspond to simulated bandwidth of 0.65 GHz. Table 1 shows the detailed performance of the array antenna with the in-phase superstrate. It can be seen that, with the integration of the in-phase superstrate into the array antenna, the impedance bandwidth of the array antenna has been widened by as much as 44% compared to the array antenna used as the reference antenna.

Figures 15(a) and (b) show the results of the radiation patterns of the array antenna with the AMC ground plane at 5.2 GHz for the E-field and H-field, respectively. The array antenna has a maximum gain of 3.95 dBi in the direction of 344° with an HPBW of 62.1°. Similarly, Figures 16(a)–(b) show the radiation pattern of the array antenna with the AMC ground plane at 5.8 GHz. The maximum gain achieved is 5.61 dBi with a HPWB of 57° in the direction of 350°. The gain is low due to the distribution of the gain over a wide bandwidth of the frequency range. Additionally, the radiation pattern of the E-field and H-field for the case of the array antenna with the in-phase superstrate
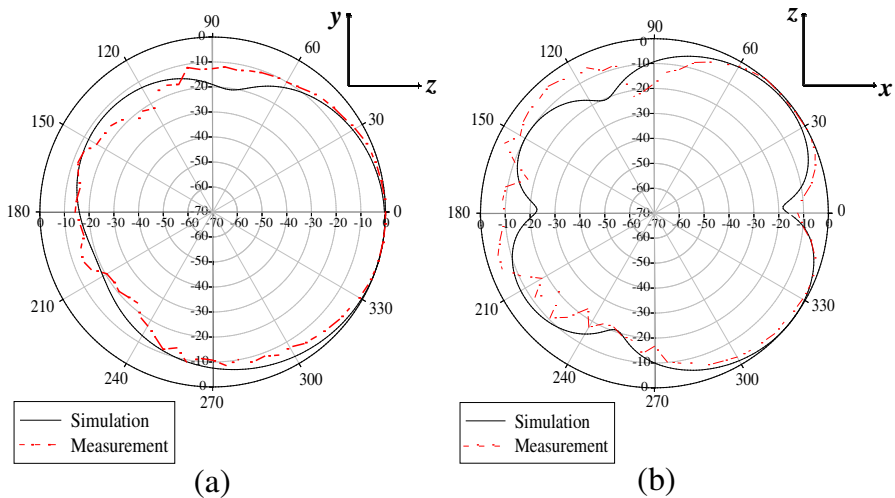

Figure 15. The simulated and measured results of the return loss curve for the array antenna with the AMC ground plane at 5.2 GHz for the (a) E-field and (b) H-field, respectively.

is shown in Figures 17(a) and (b), respectively. The array antenna exhibits a maximum gain of 7.27 dBi in the direction of 5° with a HPBW of 71.8°.
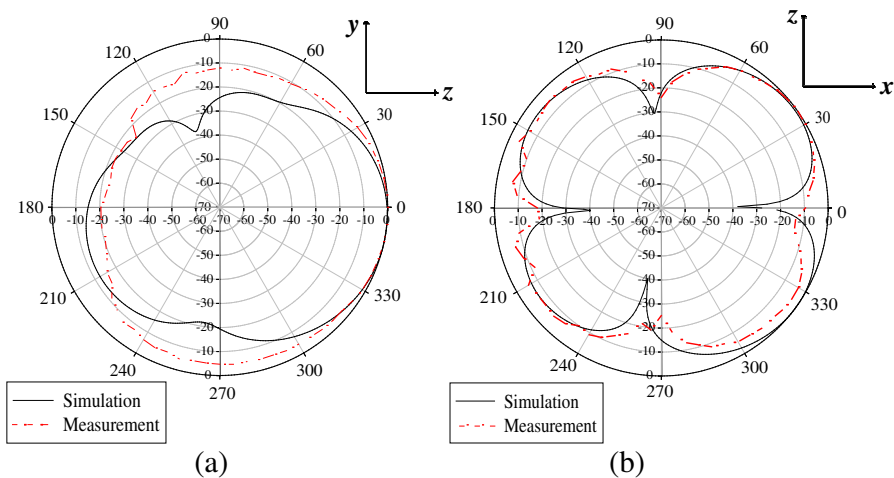

Figure 16. The simulated and measured results of the radiation pattern for the array antenna with the AMC ground plane at 5.8 GHz for the (a) E-field and (b) H-field, respectively.
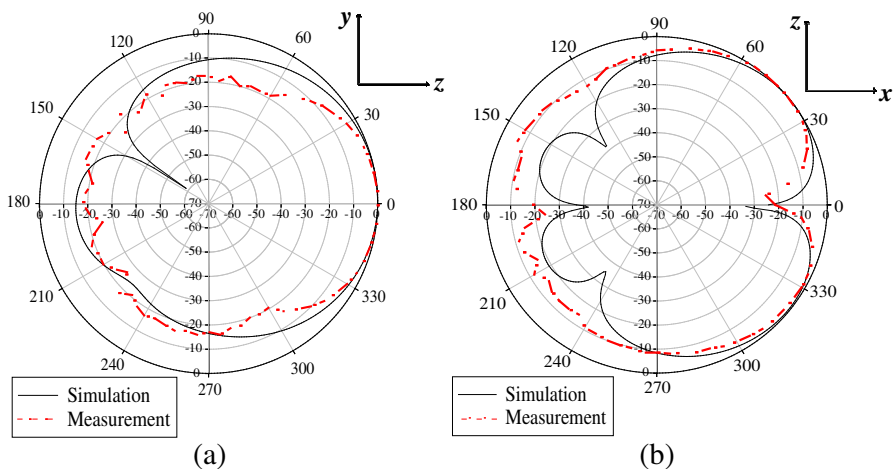

Figure 17. The simulated and measured results of the return loss curve for the array antenna with the in-phase superstrate at 5.8 GHz for the (a) E-field and (b) H-field, respectively.

Table 1. Antenna performance.

Parameter	Array antenna	AMC ground plane with array antenna		In-Phase superstrate with array antenna
		5. 2 GHz	5.8 GHz	
Percentage Bandwidth (%)	7.70	31.53		10.94
Gain (dBi)	6.26	3.95	5.61	7.27
Efficiency (%)	66.88	75.99		71.19

Table 1 shows the summary of the performance for the array antenna, the array antenna with the AMC ground plane, and the array antenna with the in-phase superstrate. Incorporation of the AMC ground plane and in-phase superstrate achieves a wide percentage bandwidth of 31.53% and 10.94%, respectively, compared with the reference antenna's bandwidth of 7.70%. It is also noted that the simulated efficiency is improved for both structures. The in-phase superstrate, in particular, increases the reference antenna gain by 1 dB.

5. CONCLUSION

The performance analyses of an AMC ground plane and an in-phase superstrate on an array antenna are presented in this paper; no such analyses have been conducted before in the literature. The implementation of an AMC ground plane reduced the antenna size while improving its efficiency. Also, the integration of the in-phase superstrate into the antenna improved the gain to 1 dB. The existence of an air gap limits the maximum gain achievable for both cases (array antenna with an AMC ground plane and with an in-phase superstrate). The air gap significantly affects the array antenna with the AMC ground plane compared to the one with an in-phase superstrate). A 0.5 mm air gap is the optimum air gap for both substrate structures, which allows for achieving the minimum possible thickness with a good tolerance for the antenna performance.

REFERENCES

1. Chen, X., J. Chen, C. Liu, and K. Huang, "A genetic metamaterial and its application to gain improvement of a patch antenna," *Journal of Electromagnetic Waves and Applications*, Vol. 26, Nos. 14–15, 1977–1985, 2012.

2. Deng, J. Y., L. X. Guo, and J. H. Yang, "Narrow band notches for ultra-wideband antenna using electromagnetic band-gap structures," *Journal of Electromagnetic Waves and Applications*, Vol. 25, Nos. 17–18, 2320–2327, 2011.

3. Zarifi, D., H. Oraizi, and M. Soleimani, "Improved performance of circularly polarized antenna using semi-planar chiral metamaterial covers," *Progress In Electromagnetics Research*, Vol. 123, 337–354, 2012.

4. Zhang, F., V. Sadaune, L. Kang, Q. Zhao, J. Zhou, and D. Lippens, "Coupling effect for dielectric metamaterial dimer," *Progress In Electromagnetics Research*, Vol. 132, 587–601, 2012.

5. Yan, S. and G. A. E. Vandenbosch, "Increasing the NRI bandwidth of dielectric sphere-based metamaterials by coating," *Progress In Electromagnetics Research*, Vol. 132, 1–23, 2012.

6. Zhang, Y., B. Z. Wang, W. Shao, W. Yu, and R. Mittra, "Artificial ground planes for performance enhancement of microstrip antennas," *Journal of Electromagnetic Waves and Applications*, Vol. 25, No. 4, 597–606, 2011.

7. Costa, F. and A. Monorchio, "Multiband electromagnetic wave absorber based on reactive impedance ground planes," *IET Microwaves, Antennas & Propagation*, Vol. 4, 1720–1727, 2010.

8. Li, L., S. Lei, and C. H. Liang, "Ultra-low profile high-gain Fabry-Perot resonant antennas with fishnet superstrate," *Journal of Electromagnetic Waves and Applications*, Vol. 26, Nos. 5–6, 806–816, 2012.

9. Li, Y. and K. P. Esselle, "Small EBG resonator high-gain antenna using in-phase highly-reflecting surface," *Electronics Letters*, Vol. 45, 1058–1060, 2009.

10. Guo, W., L. He, B. Li, T. Teng, and X. Sun, "A wideband and dual-resonant terahertz metamaterial using a modified SRR structure," *Progress In Electromagnetics Research*, Vol. 134, 289–299, 2012.

11. Segovia-Vargas, D., F. J. Herraiz-Martínez, E. Ugarte-Muñz, L. E. García-Muñoz, and V. González-Posadas, "Quad-frequency linearly-polarized and dual-frequency circularly-polarized microstrip patch antennas with CRLH loading," *Progress In Electromagnetics Research*, Vol. 133, 91–115, 2012.

12. Alam, M. S., M. T. Islam, and N. Misran, "A novel compact split ring slotted electromagnetic bandgap structure for microstrip patch antenna performance enhancement," *Progress In Electromagnetics Research*, Vol. 130, 389–409, 2012.

13. Tiang, J. J., M. T. Islam, N. Misran, and J. S. Mandeep, "Circular microstrip slot antenna for dual-frequency RFID application," *Progress In Electromagnetics Research*, Vol. 120, 499–512, 2011.

14. Foroozesh, A. and L. Shafai, "Application of combined electric- and magnetic-conductor ground planes for antenna performance enhancement," *Canadian Journal of Electrical and Computer Engineering*, Vol. 33, 87–98, 2008.

15. Dewan, R., S. K. A. Rahim, S. F. Ausordin, H. U. Iddi, and M. Z. Z. A. Aziz, "*X*-polarization array antenna with parallel feeding for WiMAX 3.55 GHz application," *IEEE International RF and Microwave Conference*, 368–372, 2011.

16. Kordalivand, A. M., and T. A. Rahman, "Broadband modified rectangular microstrip patch antenna using stepped cut at four corners method," *Progress In Electromagnetics Research*, Vol. 137, 599–619, 2013.

17. Mohamadi Monavar, F. and N. Komjani, "Bandwidth enhancement of microstrip patch antenna using Jerusalem cross-shaped frequency selective surfaces by invasive weed optimization approach," *Progress In Electromagnetics Research*, Vol. 121, 103–120, 2011.

18. Gujral, M., J. L. W. Li, T. Yuan, and C. W. Qiu, "Bandwidth improvement of microstrip antenna array using dummy EBG pattern on feedline," *Progress In Electromagnetics Research*, Vol. 127, 79–92, 2012.

19. Gebril, K. K., S. K. A. Rahim, and A. Y. Abdulrahman, "Bandwidth enhancement and miniaturization of dielectric resonator antenna for 5.8 GHz WLAN," *Progress In Electromagnetics Research C*, Vol. 19, 179–189, 2011.

20. Jeong, G.-T., W.-S. Kim, and K.-S. Kwak, "Dual-band Wi-Fi antenna with a ground stub for bandwidth enhancement," *IEEE Antennas and Wireless Propagation Letters*, Vol. 11, 1036–1039, 2012.

21. Wei, K. P., Z. J. Zhang, and Z. H. Feng, "Design of a dualband

omnidirectional planar microstrip antenna array," *Progress In Electromagnetics Research*, Vol. 126, 101–120, 2012.

22. Abbasi, N. A. and R. J. Langley, "Multiband-integrated antenna/artificial magnetic conductor," *IET Microwaves, Antennas & Propagation*, Vol. 5, 711–717, 2011.

23. De Cos, M. E., Y. Ávarez, R. Hadarig, and F. Las-Heras, "Flexible uniplanar artificial magnetic conductor," *Progress In Electromagnetics Research*, Vol. 106, 349–362, 2010.

24. De Cos, M. E., Y. Ávarez, and F. Las-Heras, "Enhancing patch antenna bandwidth by means of uniplanar EBG-AMC," *Microwave and Optical Technology Letters*, Vol. 53, 1372–1377, 2011.